Efficient scalar and vectorial singular beam shaping using homogeneous anisotropic media

Charles Loussert and Etienne Brasselet*

Centre de Physique Moléculaire Optique et Hertzienne, Université Bordeaux 1, CNRS, 33405 Talence Cedex, France
**Corresponding author: e.brasselet@cpmoh.u-bordeaux1.fr*

Received November 3, 2009; accepted November 9, 2009;
posted November 20, 2009 (Doc. ID 119221); published December 18, 2009

We propose and demonstrate a global and efficient approach for scalar and vectorial beam shaping based on the interaction of circularly polarized light with a single piece of homogeneous anisotropic medium. The main idea is to mimic the behavior of a two-dimensional inhomogeneous birefringent medium with a radial distribution of its optical axis. This is done by transforming an incident Gaussian beam into a conical nipple of light that further propagates along the optical axis of a *c*-cut uniaxial crystal. © 2009 Optical Society of America

OCIS codes: 160.1190, 260.1440, 260.6042, 260.1180.

The generation, propagation, and interaction with matter of light beams that possess phase (scalar) or polarization (vectorial) singularities are current topics in optics. In particular, the controlled generation of optical singularities that combines high efficiency and the use of simple optical elements is still an open issue. Besides strategies based on segmented polarizing optics within intra- or extra-cavity geometries, elegant approaches relying on a single piece of homogeneous uniaxial crystal have been proposed both for the scalar [1,2] and vectorial cases. In the latter case, let us mention the obtention of azimuthal [3] or radial [4] vectorial optical vortices, which have been recognized later as polarization eigenstates in *c*-cut uniaxial crystals [5]. However, the conversion efficiency could be as low as 50% [6], and one needs to cascade such devices in order to get higher-order singular optical structures. Such a requirement is bypassed when exploiting spatially patterned anisotropic optical elements, as shown in the scalar [7] and vectorial [8] situations. In fact, promising developments have been made using continuously patterned liquid crystal systems in two [9] or three [10] dimensions in the scalar case and also in the vectorial case where two- [8,11,12] or three- [13] dimensional strategies have been implemented. Hence, although attractive, the concept of 100% efficient phase and polarization singularities generation using a single piece of homogeneous uniaxial crystal appears hopeless and has not been demonstrated so far.

In this Letter, we show that this is possible by exploiting the analogy between the interaction of (i) a circularly polarized (CP) conical nipple of light with a *c*-cut homogeneous uniaxial crystal having its optical axis along the main propagation direction of light [see Fig. 1(a)] and (ii) a collimated CP beam at normal incidence onto a two-dimensional inhomogeneous uniaxial medium having a radial symmetry [referred to as a "radial plate"; see Fig. 1(b)]. To prove this, we introduce the optical conical nipple half-apex angle in air, θ_0, and the total phase delay between the ordinary (o) and extraordinary (e) waves at the output of the crystal in case (i),

$$\Phi = \frac{2\pi}{\lambda}\frac{L}{\cos\theta}[n_o - n_e(\theta)], \tag{1}$$

where λ is the wavelength in vacuum; L is the thickness of the crystal; $n_e(\theta)=n_\parallel n_\perp/(n_\parallel^2\cos^2\theta + n_\perp^2\sin^2\theta)^{1/2}$, with $n_\parallel$ ($n_\perp=n_o$) being the refractive indices along (perpendicular to) the optical axis of the crystal; and $\theta\simeq\theta_0/n_\perp$ is the refracted angle whose simplified expression is justified by the practical condition $\theta_0\ll 1$. Therefore, for any value of θ, case (i) possesses a radial plate analog, but with an effective thickness $L_{\text{eff}}=L/\cos\theta$ and a local birefringence $\Delta n_{\text{eff}}=n_o-n_e(\theta)$, as illustrated in Figs. 1(a) and 1(b), and $\Phi_{\text{eff}}=(2\pi/\lambda)L_{\text{eff}}\Delta n_{\text{eff}}=\Phi$ in case (ii).

Next, we notice that a radial plate illuminated by a CP beam can generate, formally with a 100% efficiency, a scalar vortex with a topological charge 2 when its total phase delay matches the half-wave-plate (HWP) condition [9], i.e., $\Phi_{\text{HWP}}=(2m+1)\pi$, where m is an integer. On the other hand, a vectorial vortex with a topological charge 1 is produced when

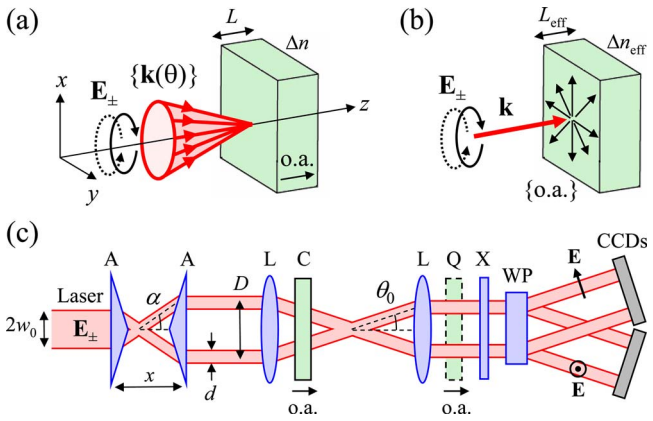

Fig. 1. (Color online) (a) CP conical nipple of light impinging on a *c*-cut calcite crystal, with o.a. being the optical axis. (b) Analog birefringent radial plate geometry. (c) Experimental setup: A, axicon; L, lens; C, calcite crystal; X—QWP, HWP, or nothing; Q, quartz crystal (used only for the vectorial case, see text); WP, Wollaston prism.

the quarter-wave-plate (QWP) condition is fulfilled, i.e., $\Phi_{QWP}=(m+1/2)\pi$ [8]. Consequently, the angle θ is the key control parameter that allows one to switch from scalar to vectorial vortex generation since it controls the value of Φ [see Eq. (1)]. Note that the value of the crystal thickness is not critical and a few millimeters are found to be convenient in practice.

The setup is described in Fig. 1(c). A conical nipple of light with a half-apex angle θ is obtained by focusing a thin ring-shaped beam with diameter D and thickness d ($d/D \ll 1$) using a lens of focal length f. The latter cylindrical nipple beam is obtained by using a pair of identical axicons with an apex angle of 140° that gives an angle of $\alpha \simeq 11.2°$ after the first axicon as shown in Fig. 1(c). The angle of incidence $\theta_0=D/(2f)$, and hence the phase delay Φ, can be controlled either by D, which is adjusted by tuning the distance x between the two axicons, or by f. In addition, d is typically defined by the incident Gaussian beam waist radius, $d \sim w_0$ [see Fig. 1(c)]. In our experiment, where a 5-mm-thick c-cut calcite crystal is used, Φ lies within the typical interval $0<\Phi<8\pi$ when using a set of focal lengths ranging from 100 to 500 mm as shown in Fig. 2(a). In Fig. 2(a), the accessible ranges for Φ are indicated by horizontal bars [14] and Φ is calculated from Eq. (1) using $n_\perp=1.656$ and $n_\parallel=1.485$ at $\lambda=633$ nm. Therefore, there are many available values of θ that ensure the HWP and QWP conditions.

The study of the HWP configuration is summarized in Figs. 2(b) and 2(c). It consists of the measurement of the power carried by the $\mathbf{c}_\pm$ components at the crystal output as a function of Φ, where the unit vectors $\mathbf{c}_\pm=(\mathbf{x}\pm i\mathbf{y})/\sqrt{2}$ refer to the CP basis. Indeed, a charge 2 phase singularity is carried by the CP field component whose spin angular momentum is flipped with respect to the incident beam, consistent with the total light angular momentum conservation [2,6].

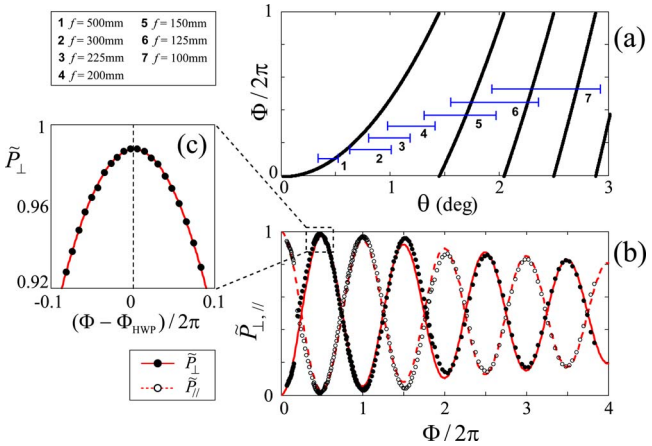

Fig. 2. (Color online) (a) Total phase delay Φ versus the internal angle of incidence θ. Horizontal bars refer to the explored range associated with the focal length f of the first lens [see Fig. 1(c)]. (b) Transfer of normalized powers between the circular components parallel ($\tilde{P}_\parallel$) and orthogonal ($\tilde{P}_\perp$) to the incident circular polarization state versus Φ: markers, experimental data; solid curves, theory. (c) Enlargement near $\Phi_{HWP}=\pi$.

Operatively, we first calibrate θ_0 versus x and then use Eq. (1) to assess the experimental value of Φ. The process of polarization conversion is shown in Fig. 2(b) where $\tilde{P}_{\parallel,\perp}=P_{\parallel,\perp}/P_0$ are the normalized powers of the parallel and orthogonal $\mathbf{c}_\pm$ field components with respect to the incident CP and P_0 is the total power. As a matter of fact, the maxima of $\tilde{P}_\perp$ correspond to the HWP condition and we obtain an efficiency of >98% when $\Phi_{HWP}=\pi$ ($m=0$) as shown in Fig. 2(c) where the solid curve corresponds to the parabolic best fit. Such a behavior agrees with the following ray optics expressions:

$$\tilde{P}_\parallel=\cos^2(\Phi/2), \quad \tilde{P}_\perp=\sin^2(\Phi/2). \tag{2}$$

We notice that Eq. (2) can be retrieved from the general formulation given by Ciattoni *et al.*, who considered the generation of a charge 2 phase singularity from a CP cylindrically symmetric beam impinging at normal incidence onto a c-cut uniaxial crystal under the paraxial approximation [2]. Indeed, by retaining a single transverse wavevector component κ in the integral expressions given by Eq. (B3) of [2], we obtain with our notations $\tilde{P}_{\parallel,\perp}=(1\pm\cos\Psi)/2$, with $\Psi=(\lambda L/4\pi)[(n_\perp^2-n_\parallel^2)/(n_\perp n_\parallel)]\kappa^2$. This gives in the small angle approximation, i.e., $\kappa=(2\pi/\lambda)\theta$, $\Psi=(\pi L/\lambda)\times(n_\perp/n_\parallel^2)(n_\perp^2-n_\parallel^2)\theta^2$. Hence we get $\Psi=\Phi$ [see Eq. (1)] and above expressions for Eq. (2) follow. However, the discrepancy between experimental data and Eq. (2) becomes significant at larger Φ. Indeed the efficiency goes down to $\simeq$75% for $m=3$ [see Fig. 2(b)]. Clearly, this is related to the finite thickness of the optical nipple in experiments, $d \neq 0$, which implies a spreading of its apex angle that should write as $\theta\pm\Delta\theta$.

The total angular spreading $\Delta\theta$ is roughly estimated by summing the two contributions arising from the first lens, $\Delta\theta_{lens}\equiv d/(2f)$, and from the diffraction, $\Delta\theta_{diff}=2\lambda/(\pi d)$, whose expression assumes a Gaussian intensity profile for the cylindrical nipple obtained after the pair of axicons. The latter assumption is validated experimentally, as shown in Fig. 3(a), where the Gaussian best fit gives $d \simeq 400$ μm.

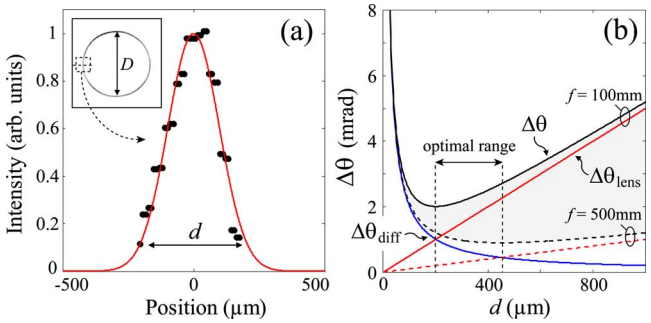

Fig. 3. (Color online) (a) Experimental intensity profile of the ring-shaped beam obtained after the pair of axicons (inset) and its cross-section fitted by a Gaussian function of waist diameter d. (b) Total ($\Delta\theta$) and diffraction ($\Delta\theta_{diff}$) and lens ($\Delta\theta_{lens}$) parts of the angular spreading versus d. The gray area corresponds to the range of values explored by $\Delta\theta$ when the focal length f is varied from 100 (dashed curves) to 500 (solid curves) mm.

Note that such a value lies within the optimal range 200–450 μm, where $\Delta\theta=\Delta\theta_{\text{lens}}+\Delta\theta_{\text{diff}}$ is globally minimized for the set of focal lengths [see Fig. 3(b)]. This emphasizes *a posteriori* the optimized character of the designed experiment. As a result, we can fit the $\tilde{P}_{\parallel,\perp}$ data by Eq. (2) but replacing Φ with

$$\langle\Phi\rangle=\frac{1}{2\Delta\theta}\int_{\theta-\Delta\theta}^{\theta+\Delta\theta}\Phi(\theta')\mathrm{d}\theta', \tag{3}$$

with $\Delta\theta$ being the single adjustable parameter. We find $\Delta\theta\simeq 1.6$ mrad, which gives a satisfying agreement [see solid curves in Fig. 2(b)]. This value is consistent with the average of $\Delta\theta$ over the investigated range for f, $\langle\Delta\theta\rangle=1/(f_{\max}-f_{\min})\int_{f_{\min}}^{f_{\max}}[d/(2f)+2\lambda/(\pi d)]\mathrm{d}f\simeq 1.8$ mrad.

In the QWP configuration, the azimuthal polarization dependence of the output nipple of light is given by the azimuth $\psi=\varphi\pm\pi/4$, where φ is the polar angle in the (x,y) plane and the $\pm$ sign depends on the index m and the handedness of the input CP. Such an axially polarized beam can be converted into a radially ($\psi=\varphi$) or azimuthally ($\psi=\varphi\pm\pi/2$) linearly polarized beam by using an optically active medium that rotates the polarization plane by an angle of $\delta\varphi=\pm\pi/4$. To do so, we use a c-cut quartz crystal of thickness 2.4 mm that gives $\delta\varphi=\pi/4$ at $\lambda=633$ nm. Note that the linear birefringence of the quartz does not affect the polarization, since the beam is impinging on it at normal incidence [see Fig. 1(c)]. Therefore, when the condition $\Phi=\Phi_{\text{QWP}}$ is set, we obtain either a radial or azimuthal linear polarization depending on the spin sign of the input beam.

The experimental demonstration is done by performing the spatially resolved polarimetric analysis of the output beam. For this purpose, we measure the Stokes parameters $S_0=|E_x|^2+|E_y|^2$, $S_1=|E_x|^2-|E_y|^2$, $S_2=2\,\mathrm{Re}(E_x^*E_y)$, and $S_3=2\,\mathrm{Im}(E_x^*E_y)$ of the output beam. Their reduced values $s_i=S_i/S_0$ $(i=1,2,3)$ all range between -1 and 1 and $s_{1,2}$ are shown in Fig. 4 for $\mathbf{c}_+$ [Fig. 4(a)] and $\mathbf{c}_-$ [Fig. 4(b)] input polarization, where the solid curves correspond to the expected behavior, namely, $s_1^+=-\cos 2\varphi$ and $s_2^+=-\sin 2\varphi$ [Fig. 4(a)], and $s_1^+=\cos 2\varphi$ and $s_2^-=\sin 2\varphi$ [Fig. 4(b)]. On the other hand, the third Stokes parameter over the whole beam is $s_3=0.01\pm 0.1$, thus confirming a satisfying local degree of linear polarization whose azimuth is given by $\psi=(1/2)\arctan(s_2/s_1)$. The corresponding azimuthal and radial polarization distributions are shown in Figs. 4(a) and 4(b), respectively.

In conclusion, we showed the generation of scalar and vectorial singular beams from a CP Gaussian beam and a single piece of homogeneous uniaxial crystal, with nearly 100% conversion efficiency. This has been made possible by transforming the incident beam into a conical nipple of light, thus mimicking the behavior of a birefringent radial plate. In contrast to inhomogeneous anisotropic radial plates, the proposed technique neither requires a material patterning nor a careful manufacturing of a wavelength dependent phase delay of the optical element. Hence, this scheme identically applies whatever is the wavelength. Finally we note that the obtained singular ring-shaped beam can be further recombined into a usual vortex beam by symmetrizing the setup, using a second pair of axicons.

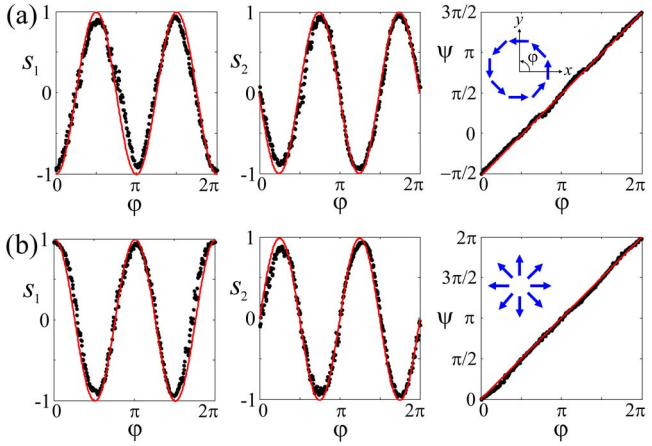

Fig. 4. (Color online) Azimuthal dependence of the reduced Stokes parameters s_1 and s_2, and polarization azimuth ψ for (a) $\mathbf{c}_+$ and (b) $\mathbf{c}_-$ polarized incident beams: markers, experimental data; solid curves, theory.

References and Notes

1. A. Volyar and T. Fadeyeva, Opt. Spectrosc. **94**, 235 (2003).
2. A. Ciattoni, G. Cincotti, and C. Palma, J. Opt. Soc. Am. A **20**, 163 (2003).
3. D. Pohl, Appl. Phys. Lett. **20**, 266 (1972).
4. K. Yonezawa, Y. Kozawa, and S. Sato, Opt. Lett. **31**, 2151 (2006).
5. P. Muys, T. Moser, and T. Feurer, J. Opt. Soc. Am. B **24**, 2627 (2007).
6. E. Brasselet, Y. Izdebskaya, V. Shvedov, A. S. Desyatnikov, W. Krolikowski, and Yu. S. Kivshar, Opt. Lett. **34**, 1021 (2009).
7. G. Biener, A. Niv, V. Kleiner, and E. Hasman, Opt. Lett. **27**, 1875 (2002).
8. S. C. McEldowney, D. M. Shemo, R. A. Chipman, and P. K. Smith, Opt. Lett. **33**, 134 (2008).
9. L. Marrucci, C. Manzo, and D. Paparo, Phys. Rev. Lett. **96**, 163905 (2006).
10. E. Brasselet, N. Murazawa, H. Misawa, and S. Juodkazis, Phys. Rev. Lett. **103**, 103903 (2009).
11. M. Stalder and M. Schadt, Opt. Lett. **21**, 1948 (1996).
12. H. Ren, Y.-H. Lin, and S.-T. Wu, Appl. Phys. Lett. **89**, 051114 (2006).
13. Y.-H. Wu, Y.-H. Lin, H. Ren, X. Nie, J.-H. Lee, and S.-T. Wu, Opt. Express **13**, 4638 (2005).
14. For a given focal length f, the lowest accessible value for θ corresponds to the contact between the pair of axicons, whereas the largest value is related to the clear aperture of the optical elements.